Journal of Catalysis 274 (2010) 273–286

Contents lists available at ScienceDirect

Journal of Catalysis

journal homepage: www.elsevier.com/locate/jcat

Synthesis, characterization, and catalytic performance of NiMo catalysts supported on hierarchically porous Beta-KIT-6 material in the hydrodesulfurization of dibenzothiophene

Dengqian Zhang, Aijun Duan, Zhen Zhao *, Chunming Xu *

State Key Laboratory of Heavy Oil Processing, China University of Petroleum, Beijing 102249, PR China

ARTICLE INFO

Article history:
Received 2 July 2010
Revised 11 July 2010
Accepted 12 July 2010
Available online 11 August 2010

Keywords:
Synthesis
Characterization
Hydrodesulfurization
Dibenzothiophene
Beta-KIT-6
Micro-mesoporous composite material
Reaction network

ABSTRACT

Micro-mesoporous composite material Beta-KIT-6 (BK) with the BEA microporous structure and cubic Ia3d mesoporous structure was synthesized and used as catalyst support for the hydrodesulfurization of dibenzothiophene. The composite material possessed both KIT-6 and Beta structures. NiMo/BK had similar acidity as NiMo/Beta and possessed more acid sites and stronger acidity than NiMo/KIT-6 and NiMo/SBA-15. NiMo/BK showed the highest dibenzothiophene hydrodesulfurization activity among all the catalysts that were studied, and the dibenzothiophene conversion on NiMo/BK was about 2–3 times that of NiMo/Al_2O_3. The acidity of NiMo/BK enhanced the activity of the direct desulfurization pathway more significantly than that of the hydrogenation pathway. Cyclohexen-1-yl-benzene was detected as intermediate of the hydrogenation pathway. NiMo/KIT-6 exhibited higher activity than NiMo/SBA-15 due to the superior mass transfer ability of the cubic Ia3d mesoporous structure.

1. Introduction

The reduction of the sulfur content in gasoline and diesel fuels has been a subject of intensive investigations in recent years. For environmental reasons, the sulfur levels must be reduced to 10 ppm in many developed countries [1,2]. To meet the stringent regulation of the sulfur content, even highly refractory molecules such as dibenzothiophene (DBT) and 4,6-dimethyldibenzothiophene (4,6-DMDBT) must be desulfurized. Due to the effects of large molecular size and steric hindrance from the alkyl substituents, it is difficult to desulfurize DBT and 4,6-DMDBT with traditional hydrotreating catalysts. In order to remove these highly refractory molecules, several approaches have been pursued, among which the development of catalyst support is of great importance [1].

Mesoporous materials with open pores are ideal catalyst supports, for the catalytic conversion of large molecules because their large pore sizes can mitigate the diffusion barrier for the reactants and products. Mesoporous materials such as MCM-41 [3], HMS [4], and SBA-15 [5] have been employed as supports for hydrodesulfurization (HDS) catalysts. Sampieri et al. [6] prepared SBA-15 and MCM-41-supported MoS_2 catalysts with various Mo loadings. MoS_2 slabs with an average length of 2.8 nm and a stacking degree of 2 were present in the pores of the SBA-15-supported catalyst. However, the relatively small mesopores in MCM-41 were blocked by the MoS_2 slabs, resulting in a lower activity than that of the SBA-15-supported counterpart [6].

Besides pore size, pore structure, e.g. pore shape and connectivity, also plays an important role in the diffusion process. Both MCM-41 and SBA-15 are two-dimensional (2D) hexagonal (p6 mm) mesostructures [7]. The unidirectional pore systems in the 2D mesostructures cause more diffusion resistance than pore system in three-dimensional (3D) mesostructure of the same pore size. Recently, Kleitz et al. [8] reported a new cubic mesoporous silica material named KIT-6, which was prepared using triblock copolymer $EO_{20}PO_{70}EO_{20}$ (P123) as the mesopore-directing agent and *n*-butanol as additive under acidic conditions. KIT-6 was reported to possess bicontinuous cubic mesostructure with large pore diameter and thick pore walls of about 8 and 3.5 nm, respectively [8,9]. Complementary pores (about 1.7 nm) connecting the two-group helical mesochannels were confirmed by TEM investigation into KIT-6 nanowire replicas [10]. Soni et al. [11] reported that KIT-6-supported Mo, CoMo, and NiMo catalysts exhibited higher activities for the conversion of thiophene than SBA-15 and γ-Al_2O_3-supported catalysts. However, just like SBA-15, pure siliceous KIT-6 material is devoid of Brönsted and Lewis acid sites [12]. This may be disadvantageous since a suitable acidity of the

* Corresponding authors. Address: 18# Fuxue Road, Chang Ping District, Beijing 102249, PR China. Fax: +86 10 69724721.
E-mail addresses: zhenzhao@cup.edu.cn (Z. Zhao), xcm@cup.edu.cn (C. Xu).

0021-9517/$ - see front matter © 2010 Elsevier Inc. All rights reserved.
doi:10.1016/j.jcat.2010.07.012

support can increase the conversion of the refractory molecules, especially of 4,6-DMDBT [13,14]. Recently, important advances in the improvement in acidity and stability of mesoporous materials have been made through synthesis of micro-mesoporous composite materials [15,16]. Many micro-mesoporous materials, including MSU-S [17], Beta-MCM-41 [18], Beta-SBA-15 [19], and mesoporous ZSM-5 [20], were synthesized and applied in the field of catalysis. Sun and Prins [13] reported that mesoporous H–Na-ZSM-5-supported Pt, Pd, and Pt–Pd catalysts exhibited much better catalytic performance for the HDS of 4,6-DMDBT than conventional H–Na-ZSM-5 or γ-Al_2O_3-supported catalysts and suggested that further improvement in the catalytic performance can be expected by tuning the acidity and pore size of the mesoporous zeolites. Beta-MCM-41 was also used as a support to prepare a supported NiW HDS catalyst [18], and the catalyst showed higher catalytic activity than a pure Al_2O_3-supported catalyst. Compared with Beta-MCM-41 and Beta-SBA-15, micro-mesoporous material Beta-KIT-6 possesses the large pore (larger than 5 nm) cubic Ia3d mesostructure which can further enhance mass transfer. This superior mass transfer property combined with the appropriate acidity makes Beta-KIT-6 more suitable for the HDS of refractory sulfur compounds. However, until now, synthesis and catalytic application of Beta-KIT-6 have, to our best knowledge, not been reported.

In this work, the novel Beta/KIT-6 composite material was successfully synthesized from zeolite Beta seeds by a two-step hydrothermal crystallization method using Pluronic P123 triblock copolymer (EO_{20}–PO_{70}–EO_{20}) and *n*-butanol. The Beta/KIT-6-supported NiMo catalysts were prepared and tested in the HDS of DBT. To clarify the effects of pore structure and support acidity on the catalytic performance, KIT-6, Beta, and SBA-15-supported NiMo catalysts were prepared and tested as well. The physicochemical properties of the pure supports and supported NiMo catalysts were characterized by various techniques, and their catalytic performances were compared with that of a conventional NiMo/Al_2O_3 catalyst. The main factors affecting the catalytic performance of Beta-KIT-6 composite-supported NiMo catalyst for the HDS of DBT were also discussed. Moreover, the reaction network for the HDS of DBT over the NiMo/BK catalyst was proposed.

2. Experimental

2.1. Preparation of the supports

Beta/KIT-6 (denoted as BK) was prepared as follows. A zeolite seed solution was prepared by adding 0.19 g of NaOH, 0.76 g of $NaAlO_2$, and 21.43 g of tetraethylorthosilicate(TEOS) into 29.45 g of an aqueous TEAOH solution (25%). The mixture of $Al_2O_3/SiO_2/Na_2O/TEAOH/H_2O$ with a molar ratio of 1.0/30/1.4/15/360 was stirred for 4 h at room temperature and then transferred into an autoclave to age for 24 h at 140 °C to obtain a zeolite Beta seed solution. An amount of 2 g of $EO_{20}PO_{70}EO_{20}$ (Pluronic P123) was dissolved in 49 g of H_2O with 27 g of 2 M hydrochloric acid at 35 °C, and 2.92 g *n*-butanol was added and the mixture was stirred for 1 h. Finally, 4.8 g TEOS and 7.9 g of zeolite seed solution (containing 22.5 mmol of SiO_2) were mixed with the P123 solution, resulting in a mixture of $Al_2O_3/SiO_2/P123/HCl/H_2O$ with a molar ratio of 1.0/60/0.92/109.8/11,700. The mixture was stirred for 24 h at 35 °C and then transferred to an autoclave for further reaction at 100 °C for 24 h. The aluminosilicate precursor was collected by filtration, dried at 100 °C for 10 h, and calcined at 550 °C in air for 6 h to remove the templates.

KIT-6 was synthesized according to the literature [8,9] using a triblock copolymer (P123) as structure-directing agent and *n*-butanol as additive. In a typical experiment, 2 g of P123 was dissolved in 57 g of distillated water and 19 g of 2 M hydrochloric acid, then 2.52 g of *n*-butanol was added under stirring at 35 °C. After stirring for 1 h, 6.42 g of TEOS was added dropwise at 35 °C, and the resulting mixture was stirred for 24 h at 35 °C. The final solution was transferred to a Teflon bottle and heated at autogeneous pressure for 24 h at 100 °C. The solid product obtained after hydrothermal treatment was filtered and dried at 100 °C. The template was removed by calcination at 550 °C in air for 6 h.

Beta zeolite was prepared in the same way as the zeolite seeds described in the BK synthesis, by adding 0.19 g of NaOH, 0.38 g of $NaAlO_2$, and 21.43 g of tetraethylorthosilicate (TEOS) to 29.45 g of an aqueous TEAOH solution (25%) to get a mixture of $Al_2O_3/SiO_2/Na_2O/TEAOH/H_2O$ with a molar ratio of 1.0/60/1.4/15/360. The mixture was stirred for 4 h at room temperature before being transferred to an autoclave for aging for 48 h at 140 °C to form zeolite Beta.

SBA-15 was synthesized using a method described elsewhere [21]. Al-KIT-6 and Al-SBA-15 were synthesized using a postsynthesis method described elsewhere [22]. A physical mixture of Beta and KIT-6 (PBK) was prepared by adding 1 g of H-Beta and 4 g of KIT-6 into 20 g of H_2O. The mixture was stirred for 4 h at room temperature and dried at 50 °C for 20 h. Beta and BK were ion exchanged with 1.0 M NH_4Cl at 80 °C for 1 h before being washed with water and calcined at 550 °C in air for 4 h. The procedure was repeated twice to achieve the final products H-Beta and H-BK.

2.2. Preparation of the catalysts

Supported NiMo catalysts were prepared by two-step incipient-wetness impregnation of ammonium heptamolybdate and nickel nitrate, the Mo precursor was impregnated first. After each impregnation step, the samples were dried at 110 °C for 12 h, and calcined at 550 °C in air for 4 h. The loadings of Ni (NiO 3.5 wt.%) and Mo (MoO_3 10 wt.%) were kept the same on all supports. For the BK-supported catalysts, samples with different Mo loadings (3, 7, 13, and 16 wt.% of MoO_3) were also prepared. A NiMo/Al_2O_3 catalyst was prepared by incipient-wetness impregnation of Al_2O_3 (Shangdong Zibo).

2.3. Characterization of the supports and the catalysts

The composite supports and catalysts were characterized by X-ray powder diffraction (XRD), scanning electron microscopy (SEM), transmission electron microscopy (TEM), N_2 adsorption, Fourier transform infrared spectroscopy with pyridine adsorption (pyridine-FTIR), and ^{27}Al magic-angle spinning nuclear magnetic resonance (^{27}Al MAS NMR). XRD patterns were recorded on an XRD-6000 diffractometer at 40 kV using Cu Kα radiation. For wide angle scans, the 2θ range was from 20° to 80° (the diffractometer was operated at 30 mA), and for small angle scans from 0.7° to 10° (the diffractometer was operated at 250 mA).

Surface areas and pore size distributions (PSD) of the samples were measured by nitrogen isotherms using a Micromeritics ASAP 2010 system. All the samples were degassed at 350 °C under vacuum prior to N_2 adsorption at −196 °C. The surface areas were calculated by using the BET model. The total volumes of micro- and mesopores were calculated from the amounts of nitrogen adsorbed at $P/P_0 = 0.98$, assuming that adsorption on the external surface was negligible compared with the adsorption in the pores. The PSD were calculated by using the Barret-Joyner-Halenda (BJH) method. Nonlocal density functional theory (NLDFT) analyses were performed to evaluate the PSD of the cubic Ia3d materials [9]. For the analyses, the kernel of NLDFT equilibrium capillary condensation isotherms of N_2 at −196 °C on silica was selected as the model isotherm (using desorption branch and assuming cylindrical pores). The micropores were determined from the *t*-plot analysis.

SEM images were obtained on a Cambridge S-360 apparatus operating at 20 kV. The silica-based samples were coated with gold before the SEM measurement. TEM images were taken from thin edges of particles supported on a porous carbon grid using a Philips Tecnai G2 F20 equipment operating at 300 kV.

The nature of the acid sites of the catalysts was determined by pyridine-FTIR on a MAGNAIR 560 FTIR instrument (Nicolet Co., US) with a resolution of 1 cm^{-1}. The samples were dehydrated at 500 °C for 5 h under a vacuum of 1.33×10^{-3} Pa, followed by adsorption of purified pyridine vapor at room temperature for 20 min. The system was then degassed and evacuated at different temperatures, and the IR spectra were recorded. The absolute amount of pyridine adsorbed on Brönsted acid sites and Lewis acid sites can be calculated using IMEC(B) = 1.67 cm/μmol, IMEC(L) = 2.22 cm/μmol described by Emeis [23].

^{27}Al MAS NMR spectra were recorded with a Bruker Avance III 500 MHz spectrometer at 130.327 MHz with a 0.9 μs pulse width, 6 μs delay time, and 12 kHz spinning speed.

2.4. Catalyst testing

The catalytic activities were studied by using DBT as the probe reactant. The reactions were carried out in a continuous fixed-bed inconel reactor (8 mm inner diameter and 400 mm in length) with 0.5 g catalyst (grain size of 0.3–0.5 mm). All catalysts were presulfided in situ with a mixture of 2 mol% CS_2-cyclohexane and H_2 at 360 °C and 4 MPa. After sulfidation, the temperature was decreased to the reaction temperature of 320 °C. Liquid reactant was fed to the reactor by a SZB-2 double-piston pump. The feed composition was 1.5 mmol cyclohexane (as solvent for DBT), 0.004 mmol dibenzothiophene, and 53.8 mmol H_2. According to reference [24], weight time was defined as $\tau = \omega_{cat}/\eta_{feed}$, where ω_{cat} was the catalyst weight and η_{feed}, the total molar flow to the reactor. The weight time (τ) was changed by varying the flow rates of the liquid and the gaseous reactants with their ratio kept at a constant value. Phenylcyclohexane (CHB) and cyclohexen-1-yl-benzene (CHEB) hydrogenation reactions were carried out at a weight time of 2.25 g min mol^{-1} and different temperatures with a feed consisting of 1.5 mmol cyclohexane, 0.02 mmol of CHB or CHEB, and 0.001 mmol DBT. All the reaction products were analyzed by offline Finnigan Trace GC/MS with a Trace Ultral gas chromatograph using a HP-5MS (30 m × 0.25 mm × 0.25 μm) capillary column and a pulsed flame photometric detector (PFPD). The products of hydrogenation of CHEB were analyzed using HP-5MS (60 m × 0.25 mm × 0.25 μm) capillary column.

The yields and selectivities should be considered as qualitative trends and not as quantitative results, because they were calculated based on the products detected by GC–MS analysis and on the C4 products that were calculated from the observed C12 to C8. Other cracking products, which were not detected, were not taken into account. For example 'cyclohexane', the possible cracking product that could not be detected, was not taken into account because cyclohexane was also used as the solvent.

3. Results

3.1. Structure of the supports and the catalysts

The KIT-6 sample showed an intense XRD peak at $2\theta = 0.88°$ corresponding to the (2 1 1) plane, a shoulder for the (2 2 0) plane, and a series of overlapping peaks for the (3 2 1), (4 0 0), (4 2 0), and (3 3 2) planes (Fig. 1A). The XRD pattern indicates that this material has a well-ordered mesoporous structure, which belongs to the bicontinuous cubic space group Ia3d [25]. The unit cell parameter a_0 of the calcined sample was calculated to be 24.6 nm, in good

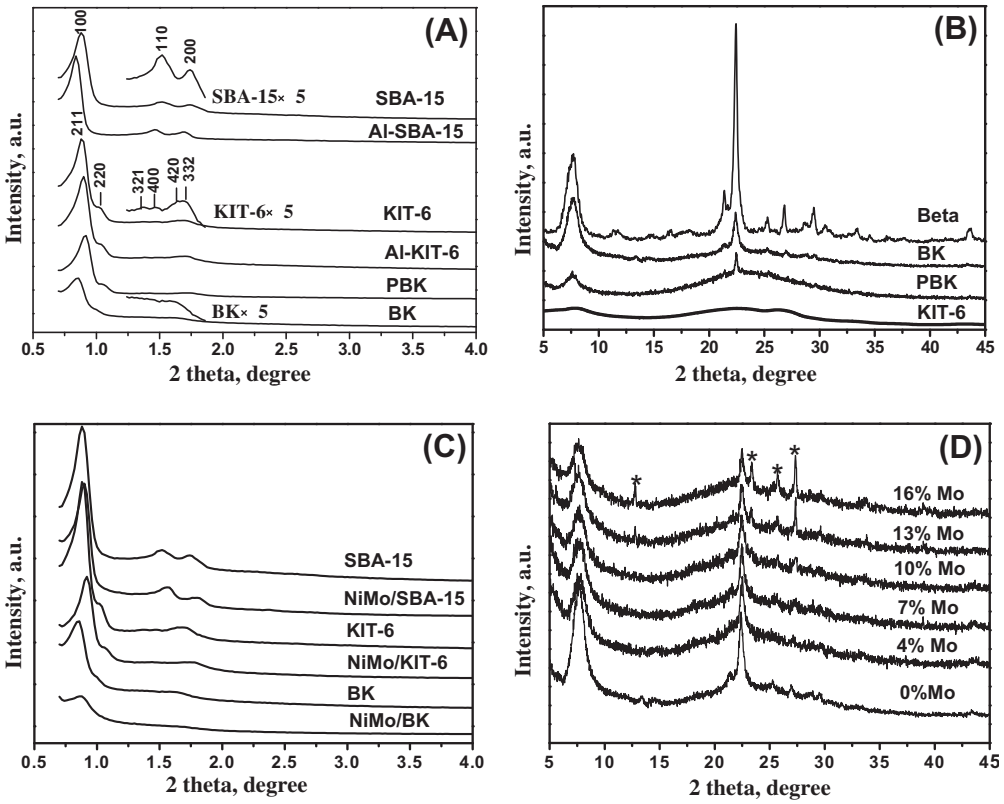

Fig. 1. XRD patterns of: (A) BK, PBK, Al-KIT-6, KIT-6, Al-SBA-15, and SBA-15 samples in the small-angle domain, (B) KIT-6, BK, PBK, and Beta samples in the wide-angle domain, (C) supports and catalysts in the small-angle domain, and (D) NiMo/BK catalysts with different Mo contents, (∗) MoO_3, JCPDS card 35-609.

agreement with the literature [8,9,25], suggesting that this mesoporous silica-based material is KIT-6 with body-centered cubic symmetry. The SBA-15 sample also gave rise to a sharp and intense peak at $2\theta = 0.88°$, corresponding to its (1 0 0) plane, and two other peaks at $2\theta = 1.52°$ and 1.74° for the (1 1 0) and (2 0 0) planes [21]. The BK sample exhibited a sharp peak at $2\theta = 0.86°$, a hump at $2\theta = 1°$, and a broad peak centered at 1.6°. These peaks agree well with the characteristics of the KIT-6 structure but have relatively low intensities. This may be due to the presence of zeolite seeds in the synthesis process, which are more difficult to assemble by the mesostructure-directing agents [19]. The small-angle XRD patterns of the Al-KIT-6 and PBK samples were similar to that of KIT-6, indicating that they have similar mesoporous structures.

The Beta zeolite possesses very intense XRD peaks at 7.6° and 22.4° (Fig. 1B), which is characteristic of zeolite Beta. The BK and PBK samples also show the same diffraction peaks as zeolite Beta, but the peak intensities are relatively weak. However, pure KIT-6 exhibits no sharp peak in the wide-angle diffraction pattern. Based on the XRD results, it is obvious that the as-synthesized material BK possesses both KIT-6 and Beta zeolite structures.

Fig. 1C shows the small-angle XRD patterns of the supported NiMo catalysts together with their corresponding support. They clearly show that all catalysts (NiMo/BK, NiMo/KIT-6, NiMo/SBA-15) exhibit the same structures as their corresponding support and indicate that the mesoporous structure was retained after metal loading.

The XRD patterns for the NiMo/BK catalysts with different metal loadings (Fig. 1D) reveal that MoO_3 is well dispersed on the BK support for loadings up to 10 wt.% since no MoO_3 peaks are detected (Fig. 1D). The absence of XRD signals indicates that the particle size of MoO_3 is below 3–4 nm [11]. In contrast, crystalline MoO_3 is present in the NiMo/BK catalysts with 13 wt.% and 16 wt.% MoO_3 loadings, as shown by a series of weak peaks in the range from 12° to 30°.

3.2. Porous properties of the supports and the catalysts

The porous properties of the supports and the catalysts were examined by N_2 adsorption–desorption isotherms at −196 °C. The textural and structural properties are shown in Table 1. The SBA-15, KIT-6, and BK supports possess high surface areas and pore volumes, consistent with reported values [9,21]. SBA-15 has micropores ($V_{mic} = 0.09\ cm^3\ g^{-1}$) from the combustion of the triblock copolymer (the mesostructure template) that was inserted into the silicate walls [7]. KIT-6 possesses a relatively large micropore volume ($V_{mic} = 0.16$) due to the presence of connecting pores between two-group helical mesochannels. BK has a relatively large V_{mic}/V_{mes} ratio, because of the contribution of Beta zeolite and has wider pore diameter and similar pore wall thickness as KIT-6. This is probably due to the stability of the mesoporous walls that are formed by assembling the zeolite primary units (contained in the zeolite seed solution) and its lower tendency toward shrinkage during the decomposition of the template.

The surface area and pore volume of the supported NiMo catalysts significantly decrease when Ni and Mo are loaded on the supports (Table 1). This decrease is more pronounced for the SiO_2-based supported catalysts than for the Al_2O_3-supported catalysts. This can be due to pore blockage caused by a low dispersion of the active metal oxide phases, as proposed by Shimada et al. [26].

N_2 adsorption–desorption isotherms of the SBA-15, KIT-6, and BK supports and their corresponding supported NiMo catalysts all show type-IV isotherms with H1-type hysteresis loop and a sharp capillary condensation step in the P/P_0 range of 0.6–0.8 (Fig. S1), a characteristic of large channel-like pores with a narrow range of PSD. In contrast, the Beta support and the NiMo/Beta catalyst have type I isotherms. In comparison, the Al_2O_3 support and the NiMo/Al_2O_3 catalyst show a H4-type hysteresis loop with a small slope in the capillary condensation regime, indicating a broad PSD. No change is observed in the type of isotherm and the shape of the hysteresis loop between the different supports and their corresponding supported catalysts. This indicates that the pore structure in the support is preserved after the deposition of the active metals. The height of the hysteresis loop decreases after Ni and Mo loadings due to the reduction of the pore volume that results from metal deposition inside the mesopores (Table 1).

The BK, KIT-6, and SBA-15 supports showed a narrow PSD, and the BK support has the largest mean pore size of 7.5 nm (Fig. 2), in agreement with the data listed in Table 1. The Al_2O_3 support possesses a weak and broad PSD, whereas no mesopores are detected in the Beta zeolite. Moreover, all catalysts showed little change in the PSD compared with their corresponding support.

Table 1
Textural properties of the supports and supported NiMo catalysts.

Samples	S_{BET}[a] ($m^2\ g^{-1}$)	V_t[b] ($cm^3\ g^{-1}$)	V_{mes}[c] ($cm^3\ g^{-1}$)	V_{mic}[d] ($cm^3\ g^{-1}$)	V_{mic}/V_{mes}	a_0[e] (nm)	d_{BJH}[f] (nm)	d_{DFT}[g] (nm)	b_w[h] (nm)	SiO_2/Al_2O_3[i]
SBA-15	699	1.03	0.99	0.09	0.09	11.6	6.4	5.7	5.2	–
KIT-6	887	1.13	1.06	0.16	0.15	24.6	6.4	5.7	6.6	–
BK	766	0.85	0.75	0.16	0.21	25.2	7.5	6.2	6.4	80
Beta	502	0.34	–	0.22	–	–	–	–		71
Al_2O_3	207	0.48	0.50	–	–	–	3.9	5.4	–	–
PBK	652	0.89	0.81	0.16	0.20	–	5.9	–	–	–
Al-KIT-6	502	0.79	0.76	0.08	0.11	24.6	6.4	–	6.6	58
Al-SBA-15	427	0.70	0.68	0.03	0.04	12	6.4	–	5.6	58
NiMo/SBA-15	441	0.80	0.80	0.01	0.01	–	6.9	5.7	–	–
NiMo/KIT-6	480	0.73	0.72	0.03	0.04	–	6.3	5.7	–	–
NiMo/BK	442	0.56	0.51	0.07	0.13	–	7.5	6.2	–	–
NiMo/Beta	339	0.26	–	0.15	–	–	–	–	–	–
NiMo/Al_2O_3	167	0.35	0.36	–	–	–	3.4	5.7	–	–
NiMo/PBK	410	0.60	0.56	0.09	0.16	–	5.2	–	–	–

[a] Calculated by the BET method.
[b] The total pore volume was obtained at a relative pressure of 0.98.
[c] Calculated using the BJH method.
[d] Calculated using the *t*-plot method.
[e] XRD unit cell parameter (a_0) was estimated from $a_0 = d_{100} \times 2/3^{1/2}$ for SBA-15 [21], and $a_0 = 6^{1/2}d_{211}$ for KIT-6 and BK [9].
[f] Mesopore diameter calculated using the BJH method.
[g] Mesopore diameter calculated by the DFT method using the kernel of NLDFT equilibrium capillary condensation isotherms of N_2 at −196 °C on silica.
[h] Wall thickness evaluated according to references [21,10]: for SBA-15 [21], $b_w = a_0 - d_{BJH}$, for KIT-6 [10] and BK, $b_w = a_0/2 - d_{DFT}$.
[i] Determined by X-ray fluorescence.

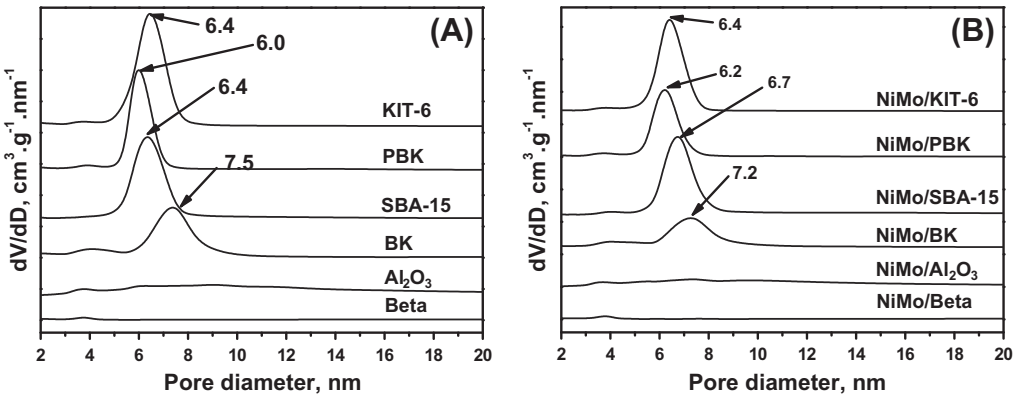

Fig. 2. Pore size distribution of: (A) supports and (B) supported catalysts.

3.3. Morphology of the supports

The SEM image shows that the SBA-15 support consists of many rice-like particles with a relatively uniform length of 1 μm (Fig. 3). The KIT-6 particles have a spherical shape with smooth surface and particles size of 2–5 μm. The BK particles are not regular in shape. This is probably due to the fact that the Beta zeolite nanocrystals are integrated into the mesoporous material particles in the synthesis process. Different from BK, the PBK sample exhibited well-crystallized Beta zeolite crystals and KIT-6 spherical-shaped particles. The Beta zeolite showed the typical crystal-like particles with size ranging from 400 to 600 nm.

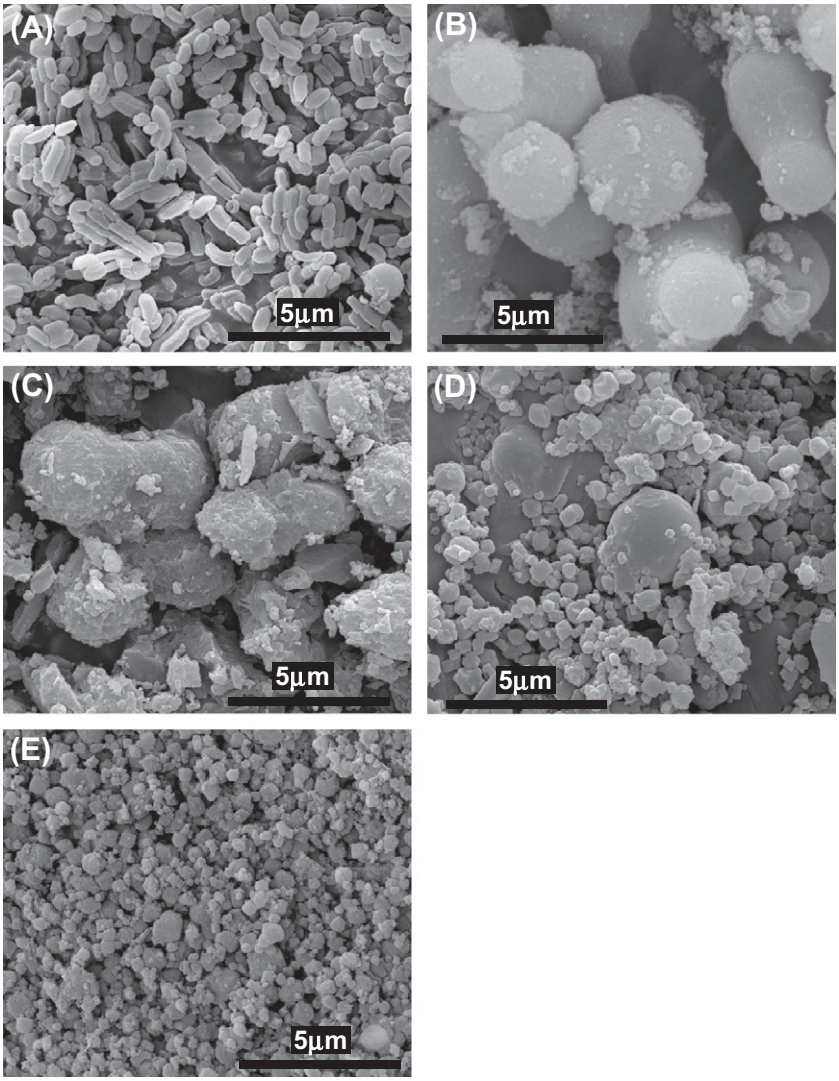

Fig. 3. SEM images of: (A) SBA-15, (B) KIT-6, (C) BK, (D) PBK, and (E) Beta.

The TEM image (Fig. 4A) of SBA-15 shows well-ordered hexagonal arrays of mesopores and confirms its 2D p6 mm hexagonal structure [21,27]. The TEM images of KIT-6 (Fig. 4B) and BK (Fig. 4C) show well-ordered cubic 3D mesoporous channels [9] and confirm that both KIT-6 and BK possess the Ia3d cubic structure. Their large pores (~7 nm) are clearly visible in the TEM images. These observations agree with the N_2 adsorption and XRD results. The higher resolution TEM (HRTEM) image of BK (Fig. 4D) show well-ordered Beta crystal lattices oriented in different directions and that the microstructure and mesostructure were overlapped in the BK sample. MoS_2 domains are seen in the HRTEM image of NiMoS/BK (Fig. 4E). They are mostly present as isolated slabs with stacks of three or four layers.

3.4. Al coordination structures

^{27}Al MAS NMR spectra of the Beta, BK, Al-KIT-6, and Al-SBA-15 supports are shown in Fig. 5. The spectrum of zeolite Beta shows two sharp peaks. The intense peak at ~57 ppm is generally assigned to tetrahedral aluminum species (AlO_4 structural unit), which are in the framework of the zeolite [19,28]. The other signal at 0 ppm is due to octahedrally coordinated extra-framework aluminum species (AlO_6 structural unit). The results indicate that most of the Al is embedded in the zeolite framework. Similar phenomenon is observed for BK. The chemical shift of tetrahedral aluminum in BK is at ~57 ppm rather than ~53 ppm, indicating that the framework aluminum species in BK is different from that in Al-incorporated mesoporous silica materials (Al-KIT-6 and Al-SBA-15). The BK sample also exhibits a signal at 0 ppm of extra-framework Al species and another peak at ~10 ppm. The latter peak can be assigned to a hexa-coordinated aluminum species with SiO group around the AlO_6 structural unit (e.g., $Q^{3[6]}$Al: $((OH)_3SiO)_3Al(OH_2)_3{\cdot}3(H_2O)$, $Q^{2[6]}$Al: $((OH)_3SiO)_2Al(OH2)_4{\cdot}2(H_2O)$, $Q^{1[6]}$Al: $((OH)_3SiO)Al(OH_2)_5{\cdot}(H_2O)$) [28,29]. These results show that extra-framework Al–O–Si species exist in the BK support and suggest that these Al–O–Si species are probably generated by the dissolution and dealumination of Beta zeolite seeds or the Beta primary units in the seed solution under the acidic condition during the synthesis of micro-mesoporous material. Al-KIT-6 and Al-SBA-15 show only one peak with a chemical shift of 53 ppm, indicating that all the Al are embedded in the mesoporous framework [30].

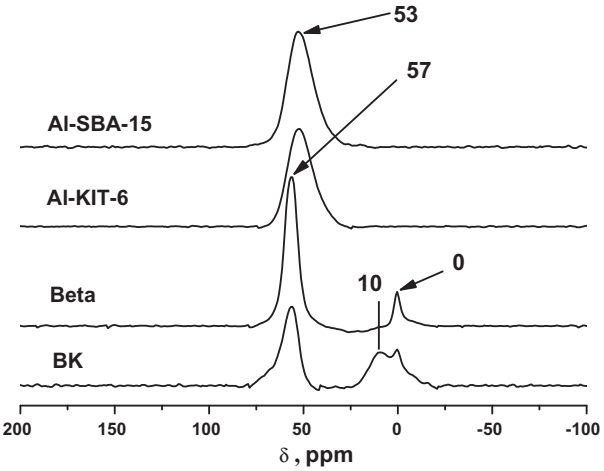

Fig. 5. ^{27}Al MAS NMR spectra of zeolite Beta, BK, Al-KIT-6, and Al-SBA-15.

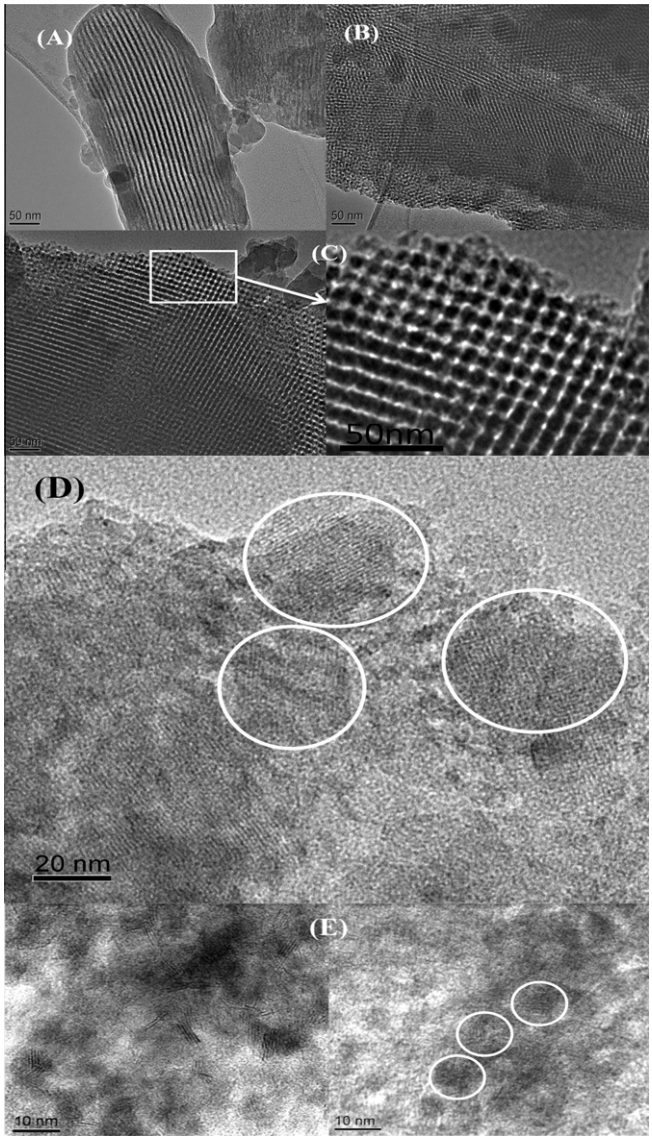

Fig. 4. TEM images of: (A) SBA-15, (B) KIT-6, (C), (D) BK, and (E) NiMoS/BK.

3.5. FTIR spectra of the supports and the catalysts

Similar to the SiO_2-based mesoporous materials (KIT-6 and SBA-15), the framework vibration spectrum of BK consists of bands centered at ~460, 810, 950, and 1030 cm^{-1} (Fig. 6). The band at 460 cm^{-1} is attributed to the Si–O–Si bending vibrations, the band at 810 cm^{-1} to the Si–O–Si symmetric stretching vibrations, and the band at 1230 cm^{-1} to the Si–O–Si asymmetric stretching vibrations. The band at 950 cm^{-1} is assigned to defective Si–OH groups [31]. Two additional bands centered at ~520 and 570 cm^{-1} in the FTIR spectra of BK and Beta are typical vibration modes for zeolite Beta (six- or five-membered rings of T–O–T (T=Si or Al) in microporous zeolites) [32]. This indicates that there are some Beta zeolite primary units in the BK material.

The acidities of the supported catalysts were investigated by the pyridine-FTIR method. Absorption bands due to adsorbed pyridine are observed in the spectra in the region of 1700–1400 cm^{-1} (Fig. 7). According to the literature [33–35], the NiMo/Al_2O_3, NiMo/KIT-6, and NiMo/SBA-15 catalysts exhibit signals due to hydrogen-bonded pyridine at 1596 cm^{-1} and pyridine adsorbed on Lewis acid sites (absorption peaks at 1446, 1575, 1609, 1622, and 1492 cm^{-1}). No Brönsted acid sites are observed in the spectra of the NiMo/Al_2O_3, NiMo/KIT-6, and NiMo/SBA-15 catalysts, as judged from the absence of the absorption band of pyridinium at

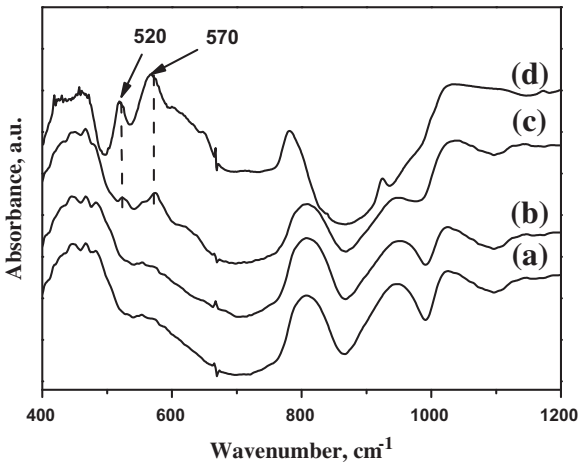

Fig. 6. FTIR spectra of: (a) SBA-15, (b) KIT-6, (c) BK, and (d) Beta.

1546 cm^{-1}. In contrast, bands at 1546 and 1639 cm^{-1} are observed in the spectra of the NiMo/Beta and NiMo/BK catalysts, suggesting that there are Brönsted acid sites in these samples. These results demonstrate that the BK-supported NiMo catalyst exhibits an acidity similar to that of the Beta-supported NiMo catalyst, but different from the acidities of the NiMo/KIT-6 and NiMo/Al_2O_3 catalysts. This is probably because both Beta- and BK-supported catalysts possess framework aluminum species (see ^{27}Al NMR results) which are responsible for the Brönsted acid sites.

Table 2 lists the acid strength distribution and the acid quantity of the catalysts. These results were calculated from the IR spectra collected from the catalysts with pyridine adsorption followed by degassing at 200 °C and 350 °C (the total amounts of acid sites were determined by the pyridine adsorption IR spectra after degassing at 200 °C, and the amounts of medium and strong acid sites were determined by the IR pyridine adsorption spectra after degassing at 350 °C). After degassing at 200 °C, the total amount of acid sites (B + L) of the NiMo/BK catalyst is similar to that of NiMo/Beta and about twice as much as that of the NiMo/KIT-6, NiMo/SBA-15, and NiMo/Al_2O_3 catalysts. This distinction is more notable (about three times) for the amounts of medium and strong acid sites (B + L after degassing at 350 °C). The NiMo/Beta catalyst possesses more strong acid sites than the NiMo/BK catalyst, especially for the Brönsted acid sites. All the Brönsted acidity in Beta is contributed by medium and strong acid sites. There is a significant proportion of weak Brönsted acid sites in NiMo/BK, although the total number of Brönsted acid sites is less than that of NiMo/Beta. This may be due to the distinctive Al chemical environment and the presence of extra-framework Si–O–Al species in the BK sample (see Fig. 5).

Table 2
Amounts of Brönsted and Lewis acid sites determined by pyridine-FTIR of the catalysts.

Catalysts	Amount of acid sites (μmol g^{-1})					
	200 °C[a]			350 °C[a]		
	L	B	L + B	L	B	L + B
NiMo/KIT-6	382	–	382	180	–	180
NiMo/BK	727	29	756	533	15	547
NiMo/SBA-15	335	–	335	198	–	198
NiMo/Beta	677	98	774	510	98	608
NiMo/Al_2O_3	358	–	358	221	–	221

[a] Degassed at 200 °C and 350 °C.

3.6. Catalyst performance in the HDS of DBT

The BK-supported NiMo catalyst showed the highest DBT conversion at all weight times, and its DBT conversion was about 2–3 times as much as that over the Al_2O_3-supported catalyst at τ = 0.75 g min mol^{-1} (Fig. 8A and B). The KIT-6-supported catalyst exhibited a lower DBT conversion than the BK-supported catalyst at all weight times, although it had larger surface area and pore volume (Table 1). This is probably due to the weaker acidity of the pure silicon KIT-6 (Table 2). In contrast, the conversions of DBT over the KIT-6-supported catalyst were higher than those over the SBA-15-supported catalyst, although they have similar textural properties (pore diameter and pore volume) and acidity. The 3D pore channel connectivity is the major factor accounting for the significant improvement in the catalytic activity. The Beta-supported NiMo catalyst exhibited the lowest conversion although it has the most acid sites (Table 2). This is probably due to the small pore size and pore volume. The Al-KIT-6-supported NiMo catalyst showed a slightly higher DBT conversion than the KIT-6 supported one at low weight times (from τ = 0.75 to 2.25), while it had slightly lower activity at high weight time (τ = 4.5) (Fig. 8A and B). The Al-SBA-15-supported NiMo catalyst showed a slightly higher DBT conversion than the SBA-15 supported catalyst at all weight times (Fig. 8A and B), but both Al-KIT-6- and SBA-15-supported NiMo catalysts had lower activities than the BK-supported catalyst (Fig. 8A and B). PBK-supported NiMo catalysts showed higher activities than NiMo/Beta and NiMo/KIT-6 at low weight time, but lower than the NiMo/BK catalyst. These results indicate that the BK material effectively integrated the superior acidity properties of Beta and the mesoporous structure of KIT-6 rather than

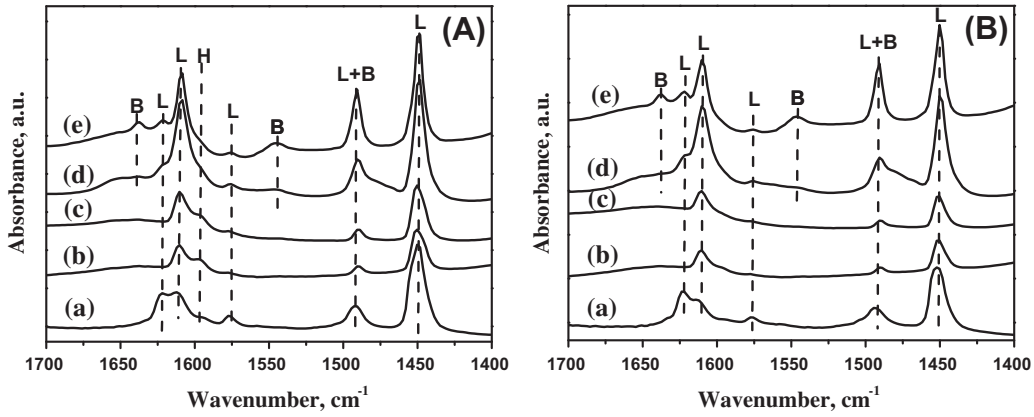

Fig. 7. FTIR spectra of pyridine adsorbed on (a) NiMo/Al_2O_3, (b) NiMo/SBA-15, (c) NiMo/KIT-6, (d) NiMo/BK, and (e) NiMo/Beta after degassing at (A) 200 °C and (B) 350 °C.

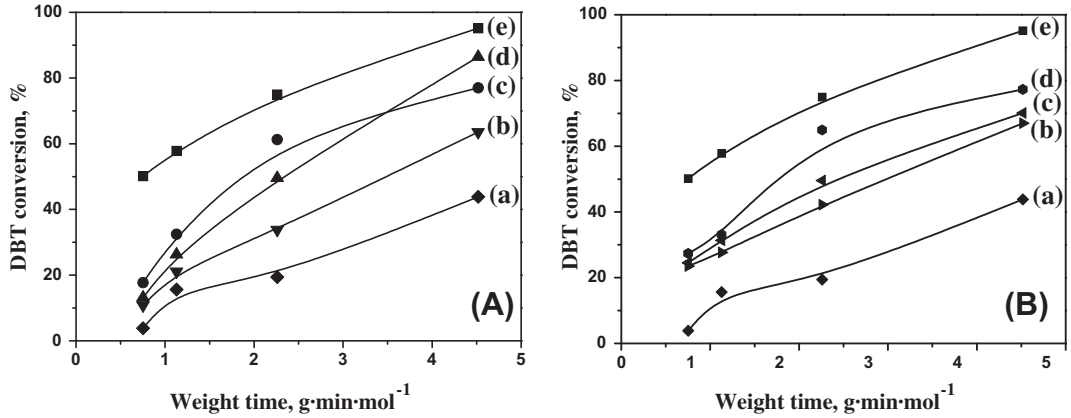

Fig. 8. Conversion of DBT in the HDS reaction over supported NiMo catalysts with various supports, Fig. (A): (a) Beta, (b) SBA-15, (c) Al_2O_3, (d) KIT-6, and (e) BK. Fig. (B): (a) Beta, (b) Al-SBA-15, (c) Al-KIT-6, (d) PBK, and (e) BK.

the separated crystal particles of Beta and KIT-6 in the PBK mixture (Fig. 3D).

The DBT conversions of NiMo/BK series catalysts with different MoO_3 loadings increased up to 10 wt.% MoO_3 loading and decreased with further increasing in the MoO_3 loading at two different weight times (Fig. 9). These results indicate that the optimal MoO_3 loading is 10 wt.%. This is probably due to the bad dispersion of the active metal of catalysts with too high MoO_3 loading. In this case the active metals aggregated to a bulk phase, which leads to a decrease of the utilization ratio and pore blocking.

The product distributions in the HDS of DBT over the BK, KIT-6, and Beta-supported catalysts are shown in Fig. 10. Five products were detected over the BK-supported NiMo catalyst: biphenyl (BP), a product of the DDS pathway [36]; tetrahydro-dibenzothiophene (THDBT), an intermediate of the HYD pathway; and CHEB, a product of direct desulfurization of THDBT, isomers of dimethyldecalin (Iso-DM-Decalin) and isomers of alkylcyclohexane (Alkyl-CH). Iso-DM-Decalin and Alkyl-CH were identified by GC–MS, as shown in Fig. S3-A and B, by a series of GC peaks with retention times from 8.53 to 9.41 min. The MS spectrum of the GC peak at 8.53 min is similar to that of Iso-DM-Decalin, (including 2,3-dimethyl-decahydronaphthalene, 1,2,-dimethyl-decahydronaphthalene, and 3,8-dimethyl-decahydronaphthalene, Fig. S4), but the positions of the methyl groups could not be determined unequivocally. GC peaks at retention times 8.74, 8.77, 8.83, and 8.89 min show similar MS spectra as the MS spectrum of the peak at 8.53 min, indicating that they are isomers of DM-Decalin (Fig. S6). The GC peak at 9.41 min shows similar MS spectrum as that of ethyldecahydronaphthalene, but the position of the ethyl group is uncertain (Fig. S5). GC peaks at 3.07–4.09 min show similar MS spectra as Alkyl-CH, indicating that the products are isomers of Alkyl-CH (Fig. S7). The yield of and selectivity to Iso-DM-Decalin reached 23% and 24%, respectively, at higher weight time (Table 3). No CHB and bicyclohexyl (BCH) were detected (Fig. S2), which are the products of the HYD pathway in the HDS of DBT over $NiMo/Al_2O_3$ [36]. The presence of Iso-DM-Decalin and Alkyl-CH in the products indicates that isomerization reactions take place in the DBT HDS reaction over NiMo/BK. Among the final products, BP was always the most abundant product, irrespective of weight time. The selectivity to BP was about 70% at low weight time and 60% at high weight time, indicating that the DDS pathway is much faster than the HYD pathway over NiMo/BK catalyst under our reaction conditions. A slow rate of hydrogenation to CHB and further isomerization to Iso-DM-Decalin and Alkyl-CH may explain the slight decrease in the selectivity of BP because the increase in the selectivities of Iso-DM-Decalin and Alkyl-CH with weight time is slightly higher than the decrease in the selectivity of THDBT.

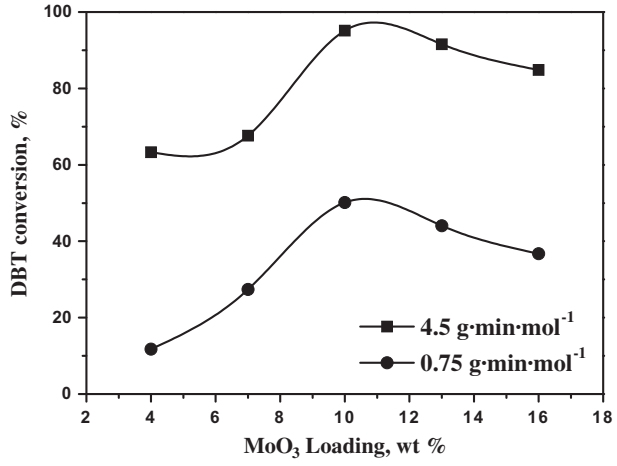

Fig. 9. Conversion of DBT in the HDS reaction over NiMo/BK catalysts with different MoO_3 loadings.

The product distribution over the Beta-supported catalyst was similar to that over the BK-supported NiMo catalyst with the former having lower DBT conversion and higher yield of cracking products of Alkyl-CH (Figs. 8 and 10C, and S2). Only three products, BP, THDBT, and CHB were observed over the KIT-6-supported catalyst (Fig. 10B, S2). The product distribution was similar to that reported for $NiMo/Al_2O_3$ [24,37]. The absence of BCH in the products indicates that complete hydrogenation of CHB is very slow over the NiMo/KIT-6 catalyst under the reaction conditions. No Iso-DM-Decalin and Alkyl-CH were detected in the products over the KIT-6-supported NiMo catalyst (Fig. S2), demonstrating that different reaction pathways or intermediates play a role during desulfurization of THDBT (an intermediate of the DBT HDS reaction).

3.7. Hydrogenation of CHEB and CHB

In order to understand the generation of Iso-DM-Decalin and the absence of CHB in the products of the DBT HDS reaction over NiMo/BK, the hydrogenation of 0.02 mmol CHEB and 0.02 mmol CHB, in the presence of 0.001 mmol DBT, was studied at different temperatures. Total CHEB conversion was observed at all reaction temperatures (Fig. 11), indicating fast kinetics under the reaction conditions. CHB and Iso-phenyl-hexadiene (Iso-PHDi) were the primary products in the hydrogenation reaction of CHEB at low temperature (Fig. 12A), and with increasing reaction temperature, Iso-DM-Decalin and Alkyl-CH became the main products. Iso-PHDi

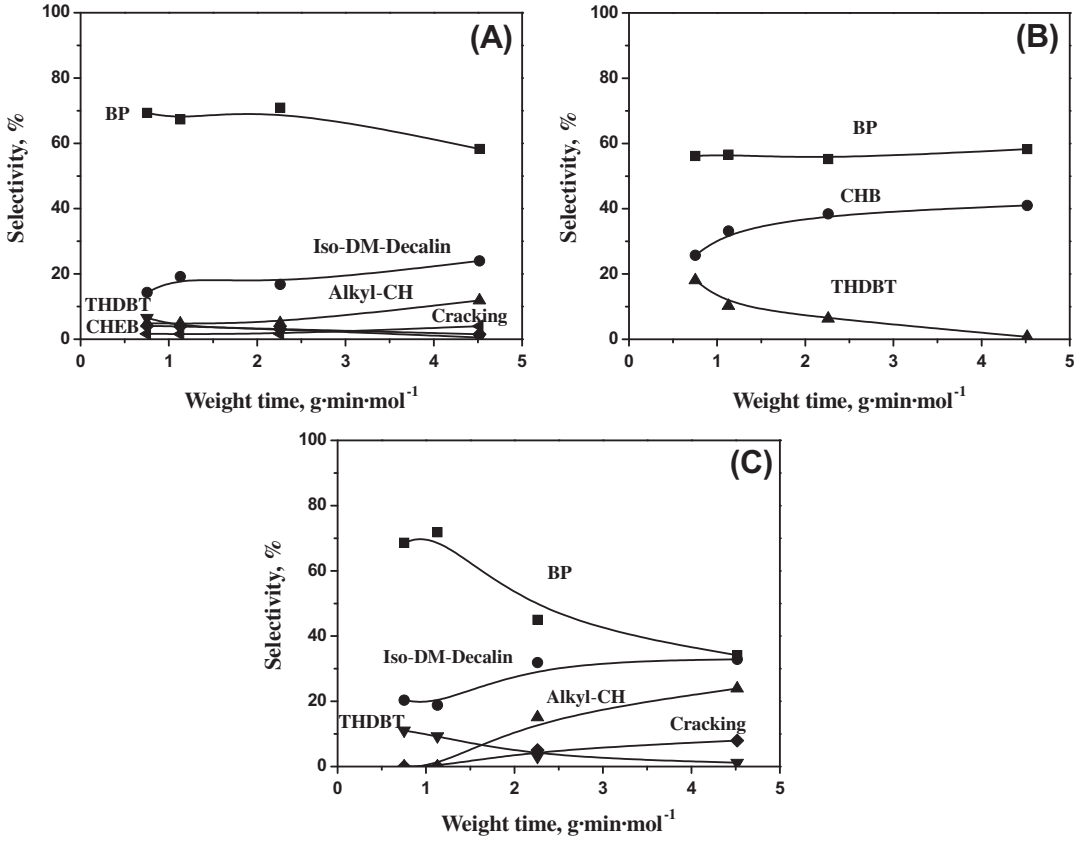

Fig. 10. Product distributions in the HDS of DBT on (A) NiMo/BK, (B) NiMo/KIT-6, and (C) NiMo/Beta catalysts as a function of weight time.

Table 3
Yields and selectivities of the final products in DBT HDS reaction on NiMo/BK, NiMo/KIT-6, and NiMo/Beta catalysts at weight time of 4.5 and 0.75 g min mol^{-1}.

Catalyst	Yield (selectivity)[a]							
	Weight time (g min mol^{-1})	BP	CHB	CHEB	THDBT	Iso-DM-Decalin	Alkyl-CH	Cracking products[b]
NiMo/BK	4.5	55.7 (58.3)	0	1.4 (1.5)	0.5 (0.52)	23.0 (24)	11.3 (11.9)	3.8 (4.0)
NiMo/KIT-6	4.5	50.9 (58.3)	35.8 (41)	0	0.65 (0.74)	0	0	–
NiMo/Beta	4.5	15.9 (34.1)	0	0	0.54 (1.2)	15.3 (32.9)	11.2 (23.9)	3.7 (8.0)
NiMo/BK	0.75	36.8 (69.3)	0	2.2 (4.1)	3.5 (6.5)	7.6 (14.3)	2.6 (4.9)	0.9 (1.6)
NiMo/KIT-6	0.75	9.3 (56.2)	4.3 (25.8)	0	3 (18)	0	0	–
NiMo/Beta	0.75	2.6 (68.6)	0	0	0.42 (11)	0.78 (20.3)	0	–

[a] Numbers in bracket represent the relative selectivity. The yield and selectivity were calculated from the GC–MS analysis results. This method is just a semi-quantitative method since the response factors of all the products in GC cannot be obtained.

[b] The cracking product yield is calculated according to the equation of $(100 - x) * 8/12 * Y_{\text{Alkyl-CH}} = x$, where x represents the yield of cracking product, $Y_{\text{Alkyl-CH}}$ is the yield of Alkyl-CH.

was identified by GC–MS, as shown in Figs. S8 and S9. The GC peak at retention time 11.51 min has similar MS spectrum as that of Iso-PHDi, but the position of the double bonds is uncertain. No CHB was detected at 320 °C. Alkyl-CH must be formed from Iso-PHDi because no CHB existed in the higher temperature range (from 290 to 320 °C), and the selectivity of Alkyl-CH increased with decreasing selectivity of Iso-PHDi. The slightly increased selectivity of Iso-DM-Decalin in the higher temperature range indicates that Iso-PHDi can also convert to Iso-DM-Decalin. It seems that the conversion of Iso-PHDi happens only at high temperatures.

The CHB hydrogenation results (Figs. 11 and 12B) indicate that CHB can convert to Iso-DM-Decalin and Alkyl-CH over the NiMo/BK catalyst. The high conversion (91%) at 320 °C shows that CHB conversion is more favorable at higher temperatures, in good agreement with the results reported by Wang et al. [38]. The conversion of CHB increases with temperature, which is probably due to the shift of the equilibrium between CHB and CHEB to CHEB at higher temperature. Moreover, more CHB is converted to Iso-DM-Decalin than to Alkyl-CH, especially in the low temperature range (Fig. 12B).

4. Discussion

The catalytic performances of HDS catalysts are affected by support and catalyst textural properties (i.e. surface area, pore size and structure, pore volume), the dispersion of the active metals [39], the acid properties of the catalysts [14,40], the reductive ability of the catalyst oxide precursors, and the nature of the support. These factors and their mutual interactions make it difficult to

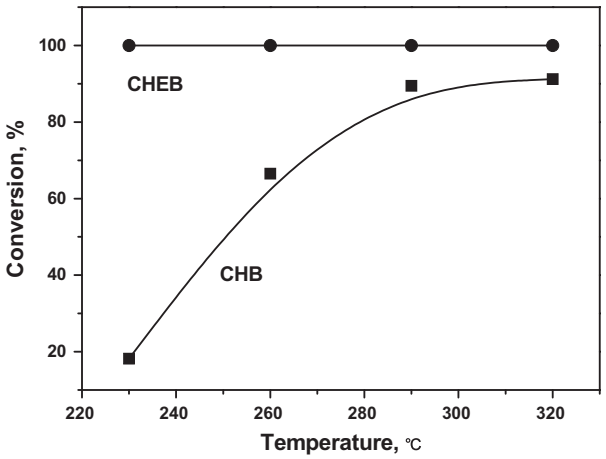

Fig. 11. Conversion of CHEB and CHB in the hydrogenation reaction over NiMo/BK catalyst as a function of temperature (0.001 mmol DBT was present during reaction).

understand the catalytic reaction mechanism. In this study, several catalysts were studied aiming at clarifying the relationship between their catalytic performances and the pore structure and the acid properties.

4.1. Effect of the pore structure on the catalytic performance for the HDS of DBT

The pore properties of catalysts are important for the catalytic conversion of reactants with large molecular size. Many efforts have been made to achieve suitable pore structure to eliminate the steric hindrance in the HDS of DBT or 4,6-DMDBT. Large pores can eliminate diffusion resistance and enhance accessibility of the active sites to reactant molecules. Because of the larger pore size, mesoporous materials (especially MCM-41 with pore size of 2–4 nm and SBA-15 with pore size of 6–10 nm) have been employed as catalyst supports for the HDS of DBT or 4,6-DMDBT [3,5]. MCM-41, with relatively smaller pore size, can generate diffusion resistance after loading of the catalytically active material. Sampieri et al. [6] reported that multilayer MoS_2 slabs loaded inside the MCM-41 pores could lead to serious limitations in the accessibility to the active sites, while this did not occur in SBA-15 because of its larger pore size. This shows that pore size of mesoporous support can affect HDS performance.

Besides the pore size of the support, the pore structure also plays an important role in the catalytic performance of HDS catalysts. In this work, two types of pure silica mesoporous materials, SBA-15 (2D-hexagonal (p6 mm) mesostructure) and KIT-6 (cubic Ia3d mesostructure), were synthesized and their corresponding supported NiMo catalysts were prepared. Both catalysts have large pore size (larger than 5 nm), possess similar textural properties (Table 1), exhibit similar PSD (Figs. S1 and S2), even have similar acidic properties (Fig. 7 and Table 2), and possess only few Lewis acid sites. However, these two catalysts exhibit different DBT HDS activities. The conversion of DBT reached 86% over the KIT-6-supported catalyst at high weight time, which is about 23% higher than that of the SBA-15-supported catalyst. To a great extent, the higher activity of the KIT-6-supported catalyst should be related to the pore structure. KIT-6 has a bicontinuous cubic structure of Ia3d symmetry and is composed of an enantiomeric pair of 3D mesoporous networks, as in the MCM-48 structure. KIT-6 also possesses complementary pores of 1.7 nm, which form interconnections between the two main channel systems [8,10]. In contrast, SBA-15 has 2D hexagonal p6mm symmetry with cylindrical pore network.

Previous studies [41,42] showed that mass transfer in the pores of the cubic Ia3d structure (MCM-48 and KIT-6) is faster than in the cylindrical pore network (MCM-41 and SBA-15) because the interwoven and branched pore structure of cubic Ia3d mesoporous materials provides more favorable mass transfer kinetics than the cylindrical pore network. This is further confirmed in this study by the better catalytic HDS performance over the KIT-6-supported catalyst than over the SBA-15-supported catalyst. Thus, on the one hand, similar to the SBA-15 support, the large pore size of KIT-6 can enhance the DBT diffusion property, but, on the other hand, KIT-6 further improves the mass transfer kinetics of DBT due to its pore structure.

4.2. Effect of acidity on the catalytic performance for the HDS of DBT

Supports or catalysts with proper acid distributions can improve the conversions of DBT and 4,6-DM-DBT [13,14]. One explanation is that acidity improves the rate of dealkylation and isomerization reactions of alkyl substituents, which may transform the refractory components into more reactive species and thus accelerate the HDS process [14]. Moreover, acidic supports may also improve catalytic activity by the creation of a second hydrogenation pathway through spillover of hydrogen atoms from the metal particles to the aromatic sulfur-containing molecules that are adsorbed on acid sites in the vicinity of the metal particles [43].

In this study, NiMo/KIT-6 and NiMo/BK catalysts were compared to investigate the effect of acidity on the activities of the HDS catalysts. XRD and TEM results (Figs. 1C and 4) showed that

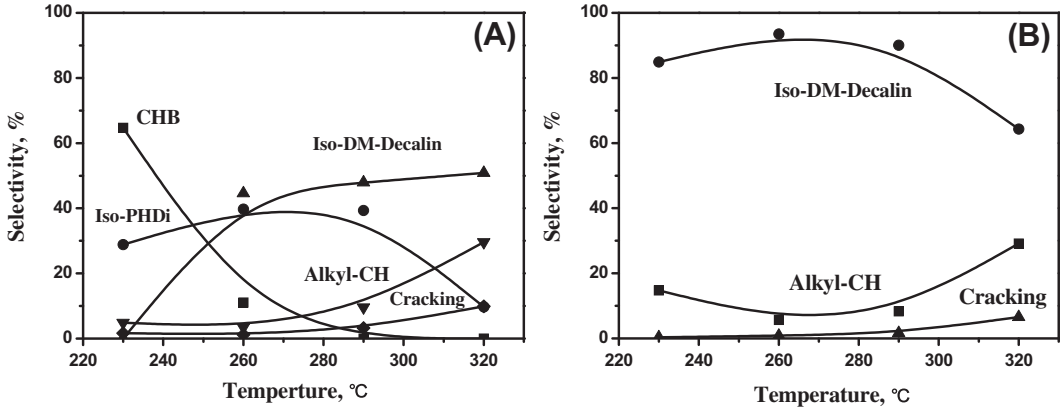

Fig. 12. Product distributions in (A) CHEB and (B) CHB hydrogenation reaction on NiMo/BK catalyst as a function of temperature.

these catalysts possess the same mesoporous structure (Cubic Ia3d mesostructure) and similar textural properties (pore size, total pore volume, and surface area, see Fig. 2 and Table 1). However, the BK-supported catalyst showed a higher DBT conversion than the KIT-6-supported catalyst at all weight times. The DBT conversion over the BK-supported catalyst was about 2.8 times higher than that over the KIT-6-supported one at $\tau = 0.75$ g min mol^{-1}. The dramatic difference in activity between the two catalysts may be mainly due to the effect of acidity. The Py-FTIR results (Table 2) show that the NiMo/BK catalyst possesses about twice as many total acid sites as NiMo/KIT-6, and even about three times when only counting the strong acid sites. Moreover, the NiMo/KIT-6 catalyst only has Lewis acid sites, while some Brönsted acid sites are also present in the NiMo/BK catalyst.

The above results show that acidity has a positive effect on the performance of the catalysts for the DBT HDS reaction. The mechanism of the effect of an acidic support on the catalytic performance of metal sulfide catalysts has been discussed by several researchers [14,44,45]. Pérot [14] considered that the positive effect of the presence of acidic components on the reactivity of 4,6-DMDBT was mainly attributed to demethylation and cracking of the C–C bond of the thiophenic ring connecting the two benzenic rings. In comparison, for DBT, the positive effect was attributed to a direct action of the acidity on the HDS active phase. Solís et al. [44] considered that the increase in the DBT HDS activity of metal sulfides by acidic supports is partly related to the improvement in their hydrogenation properties which are ascribed to electronic effects of the acidity on the metal sulfide phase. By studying the thiophene HDS behavior over a zeolite-containing catalyst, Welters et al. [45] suggested that the synergetic effect of the acidic support on the metal sulfide phase can be explained in three ways: (1) the adsorption of thiophene on the acid sites leads to a higher concentration of reactants around the metal sulfide particles, resulting in an enhanced reaction rate; (2) the high concentration of protons in close vicinity of the metal sulfide particles can lead to an acceleration of the rate-determining step in the thiophene HDS reaction and protons may also directly accelerate the C–S bond scission; and (3) the interaction between the metal sulfide particles and the protons of the acidic support may lead to the formation of a larger number of acidic SH groups on the sulfide surface, which are probably involved in the thiophene HDS reaction. Therefore, a higher concentration of SH groups can result in a higher activity. Furthermore, Rozanska et al. [46] reported that pure zeolite alone can hydrodesulfurize DBT through direct sulfur atom elimination as well as hydrogenation–desulfurization routes.

The activities of the HYD and DDS pathways of the DBT HDS reaction over the BK-supported NiMo catalyst were higher than those of the NiMo/KIT-6 catalyst, as proved by the increased yield of BP and total HYD pathway products (Table 3). The higher activity of the HYD pathway might be ascribed to the improvement in the hydrogenation properties of the catalysts, which are mainly promoted by the effect of support acidity on the metal sulfide phase and hydrogen spillover function [47]. The acceleration of the DDS pathway may be due to the presence of Brönsted acid sites which provide protons in close vicinity of the metal sulfide particles and lead to a direct acceleration of the C–S bond scission [45]. Meanwhile, NiMo/Beta exhibited a relatively lower activity than NiMo/KIT-6, although it had a large amount of acid sites. This is probably because the small pore channels of the Beta zeolite make it hard for the reactant molecules to access the active sites. Moreover, as shown in Table 3, the selectivity of BP (product of the DDS pathway) in the DBT HDS reaction over NiMo/BK and NiMo/Beta is higher than over NiMo/KIT-6 at low weight time, demonstrating that the DDS pathway was accelerated more than the HYD pathway over the BK-supported catalysts. This indicates that the acidity effects on the catalytic performance of sulfide catalysts for the DBT HDS reaction may be mainly due to the direct acceleration of the C–S bond scission by protons or to an indirect effect on the degree of stacking and thus changing the DDS versus HYD ratio [48]. The decrease in the BP selectivity (Fig. 10A and C) of NiMo/BK and NiMo/Beta at high weight time is a result of further cracking of BP over the acidic catalysts, and the decrease is more significant for the NiMo/Beta catalyst because of its stronger acidity. The lower DBT conversion and higher yield of cracking products of alkylcyclohexane over NiMo/Beta indicate that the high amount of acid sites does not further enhance the DBT HDS activity, but rather promotes undesired cracking reactions. This agrees well with the results obtained by Lee et al. [49], which showed that pure H-zeolite-supported catalysts leads to extensive cracking of the reactants.

4.3. Reaction network for the HDS of DBT over the NiMo/BK and NiMo/Beta catalysts

The reaction network for the HDS of DBT over NiMo/Al_2O_3 has been proposed by many researchers [24,50], in which DBT is mainly converted in two parallel pathways: DDS and HYD. For the DDS pathway, the C–S bond is broken by hydrogenolysis, in which DBT and hydrogen atoms on the catalyst surface react directly to form the final product BP, and further hydrogenation of BP is slow in the presence of DBT [36]. However, in the HYD pathway, DBT is first hydrogenated to form THDBT, and then THDBT is further desulfurized to form the final product CHB [24]. Wang and Prins [36] reported that CHEB was detected in the final products of the HDS of THDBT (the intermediate in the HYD pathway in the DBT HDS reaction) [36]. In their study, CHB was the only primary desulfurized product found in the THDBT HDS reaction in the absence of 2-methylpiperidine (MPi). In contrast, in the presence of MPi, CHEB emerged as a primary product. They proposed that the desulfurization of THDBT to CHB proceeds via the CHEB intermediate and that hydrogenation of CHEB to CHB is fast but can be slowed down by MPi. Thus, CHEB can be observed and become a primary product in the presence of MPi.

The product distribution of the DBT HDS reaction that we observed over NiMo/KIT-6 is similar to that observed over NiMo/Al_2O_3 by other researchers [24,50]: BP, the product of the DDS pathway, THDBT, an intermediate of the HYD pathway, and CHB a final product of the HYD pathway. However, the products over NiMo/BK indicate that Iso-DM-Decalin and Alkyl-CH are the final products instead of CHB (Fig. 10A and S2). Meanwhile, CHEB and THDBT were detected as the intermediate products of the HYD pathway. The absence of CHB in the products over the NiMo/BK catalyst may be due to the following reasons: (1) the conversion of CHB to the final products (Iso-DM-Decalin or Alkyl-CH) is very fast so that CHB cannot be observed; (2) CHEB is directly isomerized to form Iso-DM-Decalin rather than being hydrogenated to form CHB. The CHEB and CHB hydrogenation results show that CHEB reacts fast and directly converts into Alkyl-CH, Iso-DM-Decalin, and Iso-PHDi at 320 °C (Figs. 11 and 12A). However, the reaction of CHB to Iso-DM-Decalin is not so fast, especially at lower temperature (Fig. 11). Thus, the absence of CHB and the presence of Iso-DM-Decalin in the products of DBT HDS reaction over NiMo/BK is probably due to the fast reaction rate of CHEB to Iso-DM-Decalin or Alkyl-CH.

Based on the results described above, the overall DBT reaction network over the NiMo/BK catalyst is proposed in Scheme 1. Reactions 1–4, 6, and 7 are typical processes in the DBT HDS reaction over NiMo/Al_2O_3 or NiMo/KIT-6, and reactions 5, 8, 9 only happen over the acidic catalysts NiMo/BK and NiMo/Beta. For both NiMo/KIT-6 and NiMo/BK, the hydrogenation of the first phenyl ring is the rate-determining step in the HYD pathway, and the desulfurization of the partially hydrogenated intermediates is rather fast,

since the yields of these intermediates are very low (Fig. 10A and B). Reaction 6, the hydrogenation of BP to CHB, is slow because the selectivity of BP is almost constant with increasing weight time (Fig. 10A and B). Meanwhile, further cracking of BP may occur over acidic catalysts, e.g., NiMo/Beta (Fig. 10C). Reactions 5, 7, 8 and 9 have been proven by the results of hydrogenation of CHEB and CHB over the NiMo/BK catalyst (Figs. 11 and 12A and B). Alkyl-CH and Iso-DM-Decalin were detected as the primary products in the hydrogenation of CHB, indicating that reaction 7 occurs at the higher temperature (Fig. 12A and B). During the CHEB hydrogenation reaction, the higher selectivity of Alkyl-CH and Iso-DM-Decalin at the higher temperature (Fig. 12A) indicates that Alkyl-CH and Iso-DM-Decalin are mainly generated from CHEB via the Iso-PHDi intermediate (reactions 5, 8, and 9). The existence of reaction 8 indicates that some cracking reactions take place over the NiMo/BK catalyst. In this reaction, the intermediate Iso-PHDi molecule has the same number of carbon atoms as the reactant DBT molecule (12), but the product Alkyl-CH just has eight carbon atoms. Apparently four carbon atoms were lost due to cracking. The lost carbon atoms must be present in the gaseous product, but gaseous products were not analyzed. Therefore, we calculated the yield and selectivity of the cracking products according to the data of Alkyl-CH, by taking the cracking into account (for details see Table 3 and the note below Table 3). This confirms that CHEB is an intermediate in the DBT HDS reaction over NiMo/BK. Moreover, after the complete conversion of CHB, Reaction 8 may also occur in the higher temperature range, which is supported by the slight increase of the selectivity of Iso-DM-Decalin (Fig. 12A).

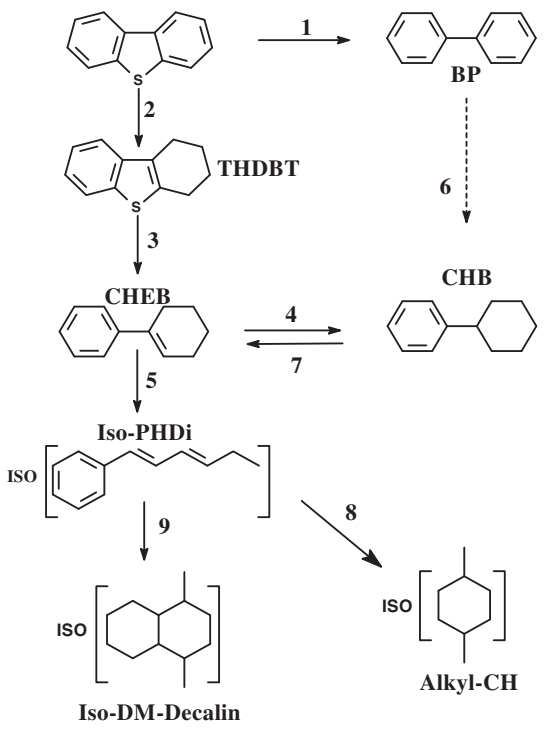

Scheme 1. Possible reaction network of the HDS of dibenzothiophene on NiMo/BK catalyst.

The presence of Iso-DM-Decalin and Alkyl-CH in the final products of the DBT HDS reaction over NiMo/BK indicates that besides the cracking reactions that have been suggested by other researchers in which CHB is cracked into benzene and cyclohexane over acidic catalysts [40,50], isomerization reactions also take place in the hydrogenation of CHEB over the NiMo/BK catalyst. The isomer-

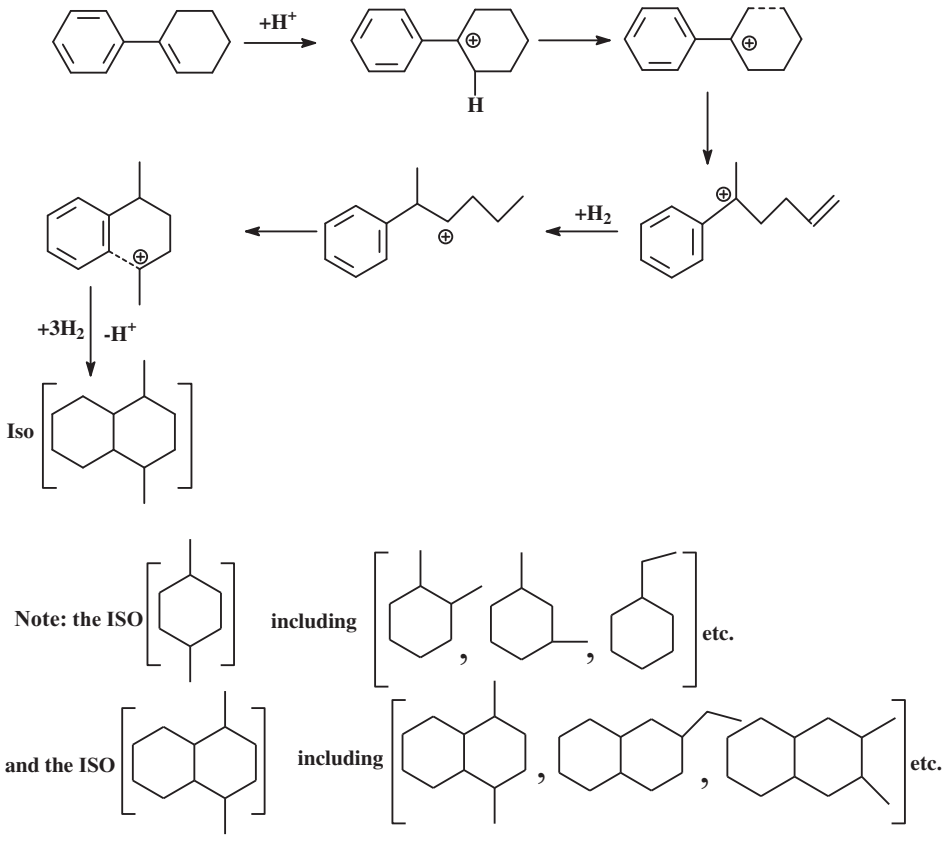

Scheme 2. Possible reaction mechanism of hydrogenation of CHEB on NiMo/BK catalyst.

ization reactions of CHEB might occur through a carbocation mechanism on Brönsted acid sites of the supports (Scheme 2). As shown in Scheme 2, CHEB first forms a carbocation at the tertiary carbon atom and then cracking occurs at β position to form hexylbenzene, which further isomerizes and cyclizes on the acid site to form the final products.

5. Conclusions

In this study, a novel micro-mesoporous composite material BK with the BEA microporous structure and cubic Ia3d mesoporous structure was successfully synthesized. The characterization results showed that the composite material possesses the same mesoporous structure as KIT-6 and contains Beta zeolite crystals. N_2 adsorption showed that the BK material has a large uniform pore size, large pore volume, and the surface area for typical mesoporous materials. A BK-supported NiMo catalyst was prepared and characterized. The cubic Ia3d mesoporous structure of BK remained after impregnation of Ni and Mo, and MoO_3 is present in highly dispersed state up to 10 wt.% loading with a crystallite size smaller than 4 nm. Similar to NiMo/Beta, the BK-supported NiMo catalyst exhibited more and stronger acidic sites than the catalysts supported on pure silica materials, such as KIT-6 and SBA-15.

The catalytic testing showed that NiMo/BK had the highest DBT HDS activity of all catalysts studied and that the DBT conversion on NiMo/BK was about 2–3 times as much as that on $NiMo/Al_2O_3$ at weight time 0.75 g min mol^{-1}. The high activity of the BK-supported catalyst may be attributed to the combination of superior mesoporous structure and large number of acid sites. The KIT-6-supported NiMo catalyst exhibited higher DBT HDS activity than the SBA-15-supported one despite its similar textural and acidic properties. This indicates that the cubic Ia3d mesoporous structure has superior mass transfer property than the 2D cylindrical pore network. Moreover, the acidity of the catalysts plays an important role in the HDS of DBT. The BK-supported catalyst possesses more acid sites and exhibits higher DBT conversion. Acidity can enhance the reaction rates of both DDS and HYD pathways, but the enhancement is more significant for the DDS pathway.

The DBT HDS reaction over the NiMo/BK catalyst follows a different network than the network over $NiMo/Al_2O_3$. Two final products, Iso-DM-Decalin and Alkyl-CH, are mainly derived from the isomerization of CHEB. They are formed via Iso-PHDi intermediates, and CHEB is an intermediate of the DBT HDS reaction.

Acknowledgments

The authors acknowledge the financial supports from the National Natural Science Foundation of China (Nos. 20876173, 20833011, and 20773163), and the Ministry of Education key project of China (No. 31). The authors are grateful to Dr. Yongsheng Chen (Energy Institute and Department of Energy and Mineral Engineering, the Pennsylvania State University) for his assistance with the English and for helpful discussions. The authors also thank Drs. Guiyuan Jiang and Jian Liu for their assistance with the English and for the preparation of data. We thank Mr. Chengyin Wang and Mr. Mingcheng Jin for their help in the evaluation of the catalytic activity.

Appendix A. Supplementary material

The supplementary information includes nitrogen adsorption/desorption isotherms of supports and supported catalysts (Fig. S1), comparison of GC peaks from the products in the HDS of DBT on NiMo/Beta, NiMo/BK and NiMo/KIT-6 at a weight time of 0.75 g min mol^{-1} (Fig. S2), GC peaks from the products in the HDS of DBT on NiMo/BK (Fig. S3), MS peaks of the GC peak at retention time 8.53 min and standard samples from the MS library (Fig. S4), MS peaks of the GC peak at retention time 9.41 min and standard samples from the MS library (Fig. S5), MS peaks of the GC peak at retention time 8.53–9.41 (Fig. S6), MS peaks of the GC peak at retention time 3.19 min and 3.27 min and standard samples from the MS library (Fig. S7), GC peaks from the products in the hydrogenation of CHEB on NiMo/BK at a weight time of 2.25 g min mol^{-1}, temperature of 320 °C and Retention Time from 5.63 to 14.55 min (Fig. S8), comparison of MS peaks of the GC (Fig. S8) peak at retention time 11.51 min and standard samples from the MS library (Fig. S9). Supplementary data associated with this article can be found, in the online version, at doi:10.1016/j.jcat.2010.07.012.

References

[1] C. Song, X. Ma, Appl. Catal. B 41 (2003) 207.
[2] A. Duan, G. Wan, Z. Zhao, C. Xu, Y. Zheng, Y. Zhang, T. Dou, X. Bao, K. Chung, Catal. Today 119 (2007) 13.
[3] U.T. Turaga, C. Song, Catal. Today 86 (2003) 129.
[4] R. Nava, J. Morales, G. Alonso, C. Ornelas, B. Pawelec, J.L.G. Fierro, Appl. Catal. A 321 (2007) 58.
[5] G.M. Dhar, G.M. Kumaran, M. Kumar, K.S. Rawat, L.D. Sharma, B.D. Raju, K.S.R. Rao, Catal. Today 99 (2005) 309.
[6] A. Sampieri, S. Pronier, J. Blanchard, M. Breysse, S. Brunet, K. Fajerwerg, C. Louis, G. Pérot, Catal. Today 107–108 (2005) 537.
[7] Y. Wan, D. Zhao, Chem. Rev. 107 (2007) 2821.
[8] F. Kleitz, S.H. Choi, R. Ryoo, Chem. Commun. (2003) 2136.
[9] T.-W. Kim, F. Kleitz, B. Paul, R. Ryoo, J. Am. Chem. Soc. 127 (2005) 7601.
[10] S. Yasuhiro, K. Tae-Wan, R. Ryong, Osamu Terasaki, Angew. Chem. Int. Ed. 43 (2004) 5231.
[11] K. Soni, B.S. Rana, A.K. Sinha, A. Bhaumik, M. Nandi, M. Kumar, G.M. Dhar, Appl. Catal. B 90 (2009) 55.
[12] A. Prabhu, L. Kumaresan, M. Palanichamy, V. Murugesan, Appl. Catal. A 360 (2009) 59.
[13] Y. Sun, R. Prins, Angew. Chem. Int. Ed. 47 (2008) 8478.
[14] G. Pérot, Catal. Today 86 (2003) 111.
[15] K. Egeblad, C.H. Christensen, M. Kustova, C.H. Christensen, Chem. Mater. 20 (2008) 946.
[16] J. Čejka, S. Mintova, Catal. Rev. Sci. Eng. 49 (2007) 457.
[17] Y. Liu, W. Zhang, T.J. Pinnavaia, J. Am. Chem. Soc. 122 (2000) 8791.
[18] S. Zeng, J. Blanchard, M. Breysse, Y. Shi, X. Su, H. Nie, D. Li, Appl. Catal. A 298 (2006) 88.
[19] Y. Han, F.-S. Xiao, S. Wu, Y. Sun, X. Meng, D. Li, S. Lin, F. Deng, X. Ai, J. Phys. Chem. B 105 (2001) 7963.
[20] M. Choi, H. Sung Cho, R. Srivastava, C. Venkatesan, D.-H. Choi, R. Ryoo, Nat. Mater. 5 (2006) 718.
[21] D. Zhao, J. Feng, Q. Huo, N. Melosh, G. Fredrickson, B. Chmelka, G. Stucky, Science 279 (1998) 548.
[22] Z. Luan, M. Hartmann, D. Zhao, W. Zhou, L. Kevan, Chem. Mater. 11 (1999) 1621.
[23] C.A. Emeis, J. Catal. 141 (1993) 347.
[24] M. Egorova, R. Prins, J. Catal. 225 (2004) 417.
[25] X. Liu, B. Tian, C. Yu, F. Gao, S. Xie, B. Tu, R. Che, L.-M. Peng, D. Zhao, Angew. Chem. Int. Ed. 41 (2002) 3876.
[26] H. Shimada, T. Sato, Y. Yoshimura, J. Hiraishi, A. Nishijima, J. Catal. 110 (1988) 275.
[27] J.S. Beck, J.C. Vartuli, W.J. Roth, M.E. Leonowicz, C.T. Kresge, K.D. Schmitt, C.T.W. Chu, D.H. Olson, E.W. Sheppard, J. Am. Chem. Soc. 114 (1992) 10834.
[28] E. Lippmaa, A. Samoson, M. Magi, J. Am. Chem. Soc. 108 (1986) 1730.
[29] L.J. Criscenti, S.L. Brantley, K.T. Mueller, N. Tsomaia, J.D. Kubicki, Geochim. Cosmochim. Acta 69 (2005) 2205.
[30] Y. Yue, A. Gédéon, J.-L. Bonardet, J.-B. DEspinose, J. Fraissard, N. Melosh, Chem. Commun. 1999 (1999) 1967.
[31] V. Umamaheswari, M. Palanichamy, V. Murugesan, J. Catal. 210 (2002) 367.
[32] P.-P. Joaquin, A.M. Johan, A.J. Peter, Appl. Catal. 31 (1987) 35.
[33] T. Kataoka, J.A. Dumesic, J. Catal. 112 (1988) 66.
[34] D. Zhang, A. Duan, Z. Zhao, G. Wan, Z. Gao, G. Jiang, K. Chi, K.H. Chuang, Catal. Today 149 (2010) 62.
[35] B. Chakraborty, B. Viswanathan, Catal. Today 49 (1999) 253.
[36] H. Wang, R. Prins, J. Catal. 258 (2008) 153.
[37] H. Kim, J.J. Lee, S.H. Moon, Appl. Catal. B 44 (2003) 287.
[38] A. Wang, Y. Wang, T. Kabe, Y. Chen, A. Ishihara, W. Qian, P. Yao, J. Catal. 210 (2002) 319.
[39] Y. Saih, K. Segawa, Appl. Catal. A 353 (2009) 258.
[40] M.V. Landau, D. Berger, M. Herskowitz, J. Catal. 159 (1996) 236.
[41] J.W. Lee, W.G. Shim, H. Moon, Micropor. Mesopor. Mater. 73 (2004) 109.
[42] K. Schumacher, M. Grün, K.K. Unger, Micropor. Mesopor. Mater. 27 (1999) 201.
[43] S.D. Lin, M.A. Vannice, J. Catal. 143 (1993) 539.
[44] D. Solís, A.L. Agudo, J. Ramírez, T. Klimova, Catal. Today 116 (2006) 469.

[45] W.J.J. Welters, V.H.J. de Beer, R.A. van Santen, Appl. Catal. A 119 (1994) 253.
[46] X. Rozanska, X. Saintigny, R.A. van Santen, S. Clémendot, F. Hutschka, J. Catal. 208 (2002) 89.
[47] X. Li, A. Wang, Z. Sun, C. Li, J. Ren, B. Zhao, Y. Wang, Y. Chen, Y. Hu, Appl. Catal. A 254 (2003) 319.
[48] M. Daage, R.R. Chianelli, J. Catal. 149 (1994) 414.
[49] Y.-K. Lee, Y. Shu, S.T. Oyama, Appl. Catal. A 322 (2007) 191.
[50] P. Michaud, J.L. Lemberton, G. Pérot, Appl. Catal. A 169 (1998) 343.